On the Stability and Safe Operation of Pod Driven Ships

Zafer Ayaz, *The Ship Stability Research Centre, Department of Naval Architecture and Marine Engineering, Universities of Glasgow and Strathclyde, UK*

Osman Turan, *The Ship Stability Research Centre, Department of Naval Architecture and Marine Engineering, Universities of Glasgow and Strathclyde, UK*

Mehmet Atlar, *School of Marine Science and Technology, University of Newcastle upon Tyne, UK*

ABSTRACT

The paper presents the enhancement of an existing 6 DOF non-linear numerical model to predict motion behaviour of a ship, which is driven by multitude of podded propulsors for high-speed, effectively combining manoeuvring and seakeeping equations in waves. The numerical model is then validated using a ROPAX and containership, for which are both driven by multi-pod propulsion systems and extensive manoeuvring and seakeeping model test data are available for both vessels. The effect of pod units on motions, including the instability and capsizing modes, are observed for these vessels, such as parametric rolling and surf-riding in extreme sea conditions, and these behaviours have been analysed. The link with design parameters and possible Risk Control Options (RCO) have been discussed and investigated. Finally dynamic intact stability characteristics of these ships are assessed and conclusions including some design alternatives in terms of safe operation of the vessels are drawn.

Keywords: Stability, azimuthing podded propulsion, safety, operation

1. INTRODUCTION

The stability characteristics of the ships are greatly influenced by the design approach to adopt their associated propulsion and steering units. This has been especially major concern by the introduction of powerful and multi-functional azimuthing podded propulsion and steering units within the last decade or so (FASTPOD, 2005, Ayaz et al., 2005). While, the sizes and power output of these propulsion/steering units are getting larger along with the speed and sizes of ships, the possible dangerous conditions related to stability and safe operations of these vessels have not been properly addressed in spite of some concerns reported in the open literature by some investigators (e.g. Van Terwisga et al., 2001, Toxepus & Loeff, 2002) as well as by the last ITTC (ITTC, 2005b).

The azimuthing pod-propulsion systems have now been well proven in terms of their propulsion performance in slow to medium speed range whilst their low speed and harbour manoeuvring performance, especially for passenger ships and ice-breakers are their biggest advantages (ITTC, 2005b). The challenge in modern transport now appears to foster the application of this technology for very large and high-speed vessels, which are also growing in numbers, to meet the demands of fast ship operators and the competitive market conditions. However, during the design stage and operation of existing pod-driven ships, many interesting and important problems

and potential danger areas have been observed from control and stability point of view. These have not been thoroughly discussed even for relatively slow speed current applications and therefore further raise questions for the high-speed applications. From model tests and actual operational experiences some of these potential danger areas have been identified such as directional stability problems due to extreme pramming of the afterbody to accommodate the pod units, effect of large steering forces created by pod drives on roll motion in heavy seas and/or excessive steering actions imposed by autopilot in calm water and the wear and tear of the bearings and steering engine caused by these activities in heavy seas (ITTC, 2005, Van Terwisga et al., 2001, Toxepus & Loeff, 2002).

Amongst a number of research studies in this area, two large European wide research projects have been undertaken to address and produce solutions to aforementioned and many other design and operational problems of pod-driven ships (OPTIPOD, 2002, FASTPOD, 2005). As part of these research studies, an existing in-house 6 DOF non-linear numerical model has been enhanced with inclusion of propulsion and steering actions of the pod drives and used as an analysis tool to investigate some of the above mentioned stability problems of pod-driven ships (Ayaz et al., 2004, 2005).

Within the above framework this paper present the enhancement of an existing 6 DOF non-linear numerical model, which predicts the combined manoeuvring and seakeeping behaviour of a ship, to include the effect of multiple number of pod units in low and high speed operating conditions. The enhanced numerical model has been validated using the extensive manoeuvring and seakeeping model test data available for a high speed ROPAX and container vessel developed in FASTPOD project. The study on current paper has focus on the possible threats to stability in relation to the changes in design to accommodate pod-structure. The effect of pod units on motions and the instability and capsizing modes observed for these vessels, such as parametric rolling and broaching-to associated with surf-riding in extreme sea conditions, have been analysed. The link with design parameters and possible RCOs (Risk Control Options) has been discussed. Finally dynamic intact stability characteristics of these ships are assessed and conclusions and design alternatives for safe operation of these vessels are identified.

2. NUMERICAL MODEL

2.1 Conventional mathematical model

The current numerical model, which was originally developed to identify the instability/capsizing limits of a ship driven by conventional propulsion system in astern seas, is a non-linear 6-DOF mathematical model and it allows a straightforward combination between the seakeeping and manoeuvring modes of vessel behaviour whilst accounting for extreme motions (Ayaz et al, 2006).

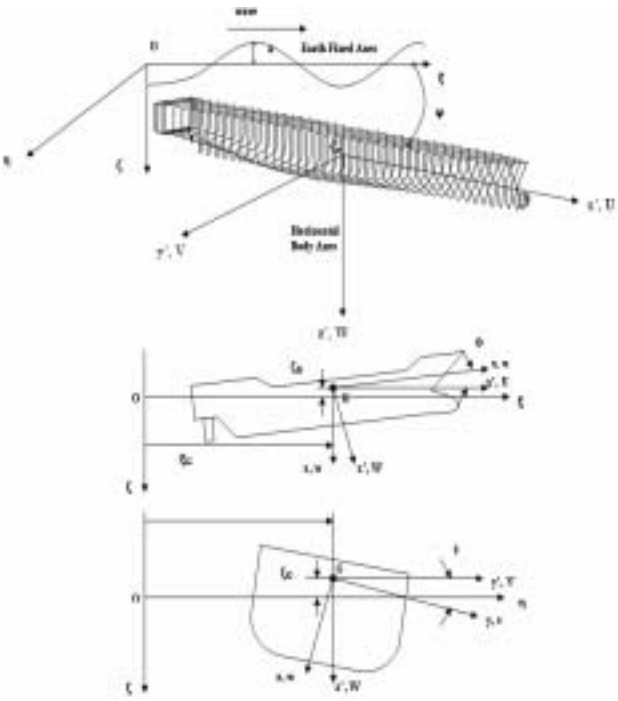

Figure 1 The axis system of numerical model.

The equations of motion have been derived using the relationship amongst three different co-ordinate axes system, namely: horizontal body axes, body axes and earth fixed axes systems represented by *G-x'y'z'*, *G-xyz*, 0-$\xi\eta\zeta$, respectively. The relationship between them is illustrated in Fig. 1 where *x*, *y*, *z* represent linear motions, *u*, *v*, *w* are linear velocities, *p*, *q*, *r* are angular velocities and φ, θ, ψ are Euler angles of rotations. By applying Newton's 2nd. law the equation of motions are expressed in standard six degrees of freedom in terms of the linear (surge, sway, heave) motions in (1) and rotational (roll, pitch and yaw) motions in (2), respectively, along with the external forces as below:

$$\begin{aligned} m(\dot{U}-VR) &= -\iint_S p\mathbf{n_X}\,dS + X_H - F_N\sin\delta \\ &\quad + (1-t_p)\rho n^2 D^4 K_T \\ m(\dot{V}+UR) &= -\iint_S p\mathbf{n_Y}dS + \rho U\int_{\Gamma_X}\Phi_D n_Y ds \\ &\quad + Y_H - (1+a_H)F_N\cos\delta \\ m\dot{W} &= -\iint_S p n_Z\,dS + \rho U\int_{\Gamma_X}\Phi_D\mathbf{n_Z}ds + Z_H \end{aligned} \tag{1}$$

$$\begin{aligned} &(I_{xx}\cos^2\theta + I_{yy}\sin^2\theta)\dot{P} = -\iint_S p(\mathbf{r}\times\mathbf{n_{YZ}})dS \\ &+\rho U\int_{\Gamma_X}\Phi_D(\mathbf{r}\times\mathbf{n_{YZ}})ds + K_H + (1+a_H)z_R F_N\cos\delta \\ &I_{yy}\dot{Q} = -\iint_S p(\mathbf{r}\times\mathbf{n_{ZX}})dS + \rho U\int_{\Gamma_X}\Phi_D(r\times n_{ZX})ds \\ &\quad + M_H \\ &(I_{xx}\sin^2\theta + I_{zz}\cos^2\theta)\dot{R} = -\iint_S p(\mathbf{r}\times\mathbf{n_{XY}})dS \\ &+\rho U\int_{\Gamma_X}\Phi_D(\mathbf{r}\times\mathbf{n_{XY}})ds + N_H - (1+a_H)x_R F_N\cos\delta \end{aligned} \tag{2}$$

where, *U*, *V*, *W* are surge, sway, heave linear velocities, *Q*, *P*, *R* are roll, pitch, yaw angular velocities in horizontal body axes system and I_{xx}, I_{yy}, I_{zz} are roll, pitch, yaw moments of inertias, respectively.

In (1) and (2), the first terms in the right-hand side of the equations in including pressure term p, correspond to the incident (or Froude-Krylov) component of the wave-excitation forces/moments including hydrostatic forces. These are calculated on the hull by integrating pressure *p* up to the instantaneous wave surface together with the kinematic relations involving **n** is normal vector and **r×n** is vector fixed with respect to centre of gravity. Here, he calculation of hydrostatic forces is of great importance to identify the dangerous conditions presented in §3. The hydrostatic forces and moments can be obtained by integrating the pressure, *p* over the entire wetted surface of the ship. The hydrostatic pressure *p* including that of a sinusoidal wave ζ_w at any time and position ξ in the earth fixed axes is given by:

$$\begin{aligned} p &= (\zeta_G - x'\theta + z') - \rho g a e^{-kd} \\ &\cos\left(k(\xi_G + x'\cos(\psi) - y'\sin(\psi) - ct)\right) \end{aligned} \tag{3}$$

with

$$\begin{aligned} \zeta_W &= -\zeta_G + x'\theta \\ &\quad + a\cos\left(k(\xi_G + x'\cos(\psi) - y'\sin(\psi) - ct)\right) \end{aligned} \tag{4}$$

where *a* the amplitude of wave, *c* the phase velocity of wave and *d* the draft of the ship. Using the above expressions in Gauss theorem, the Froude-Krylov forces can described with respect to the horizontal body axes in the form of heave, roll and pitch motion which include restoring terms as follows:

$$\begin{aligned} Z'_{F.K}(\zeta_G,\theta,\psi,\varphi) &\equiv -\iiint_V \frac{\partial p(F.K)}{\partial z'}dV \\ K'_{F.K}(\zeta_G,\theta,\psi,\varphi) &\equiv -\iiint_V \left[y_B'\frac{\partial p(F.K)}{\partial z'} - z_B'\frac{\partial p(F.K)}{\partial y'}\right]dV \\ M'_{F.K}(\zeta_G,\theta,\psi,\varphi) &\equiv -\iiint_V \left[z'\frac{\partial p(F.K)}{\partial x'} - x'\frac{\partial p(F.K)}{\partial z'}\right]dV \end{aligned} \tag{5}$$

where Z', K' and M' are heave, roll and pitch Froude-Kyrlov forces including hydrostatic terms in horizontal body axes, respectively (F.K denotes Froude-Kyrlov), (y_b', z_b') the centre of buoyancy of the immersed section at each instant. As shown in (5), these forces are calculated as parameter of the Euler angles and

vertical position of centre of gravity of ship on wave (ζ_G) at each instant for instantaneous wave surface.

The second-term in (1) and (2) involving Φ_D corresponding to the diffraction forces and Γ_x denotes the contour of section under the still water free surface, which is obtained as disturbance forces using Ohkusu's low encounter frequency slender body theory where for motions in the astern seas conditions, while strip theory has been used for other conditions (Ayaz et. al, 2006). Since the assumption of relatively comparable wave length to ship length ratio in calculation of incident (Froude-Kyrlov) and diffraction forces, the current numerical model is more suited to long-crested waves than short-crested waves.

The third terms represented by subscript H indicate hull (manoeuvring) forces, moments, which are obtained using well-known MMG (acronym for Japanese Manoeuvring Group, Inoue et al, 1981) method. The fourth terms involving F_N and K_T denote conventional rudder forces and propulsion forces in surge motion, for the latter where: F_N, the rudder normal force; a_H, rudder–to-hull interaction coefficient, x_H, the longitudinal coordinate of the point of action of the rudder to hull interaction force, x_R, z_R, longitudinal and vertical coordinates of the rudder's centre of pressure, respectively; K_T , the thrust coefficient; D, the propeller diameter, n, the propeller rate of rotation; and δ, the steering or rudder angle. Although the above equations apply to a vessel to be driven by podded propulsors, here, the notations for the steering/propulsion used follows the similar notations for the conventional rudder/propulsor for the sake of convenience. The more detailed descriptions of equations of motions and other components of the mathematical model are given in (Ayaz et al, 2005, 2006).

The left hand sides of the non-linear equations (1) and (2) contain 12 variables. Those variables along with the helm (autopilot) and positions of ship on wave can be written as:

$\boldsymbol{X}$: State Vector x ∈ $|\mathrm{R}''$

$$\mathbf{X}:\left(\zeta_G,\xi_G,x,y,z,u,v,w,p,q,r,\varphi,\theta,\psi,\delta\right)^T \qquad (6)$$

where ξ_g represent longitudinal position of centre of gravity of ship on wave, respectively and δ is the helm angle. Equations (1), (2), (3) yield to (4) in the matrix form of 2nd. Order classical motion equations as follows:

$$\begin{aligned}&(\mathbf{M}+\mathbf{A})\ddot{X}(t)+\mathbf{B}(X)\dot{X}(t)+\mathbf{C}(X)X(t)+\\&\int_0^\infty K_{ij}(t)V_j(t-\tau)d\tau=\mathbf{F}(\zeta_w,X(t),\dot{X}(t),\ddot{X}(t))\end{aligned} \qquad (7)$$

where, **M** is inertia mass/moment inertia matrix, **A** is added mass/moment inertia matrix, **B** is damping coefficients matrix, **C** is restoring coefficients matrix, **F** is external force vector and ζ_w is wave amplitude. Here, the forth term in the left-hand side of (4) represents "so-called" memory effect term incorporating the frequency-dependent vessel motion related terms (radiation forces/moments) into (4). The impulse response function (K_{ij}) will be solved from added mass and damping data and the convolution integral given in (7) then evaluated for each term in the equations of motion at each time step during the simulation. In this study, well-known 2-D strip theory is used for the calculation of radiation forces.

Finally, the control term introduced in (6) for helm angle is obtained by employing the PID (Proportional-Integral-Differential) control terms in equations of motions based on the following:

$$\delta_R+t_r\dot{\delta}_R=K_R(\psi-\psi_R)+K_P\dot{\psi}+K_i\int_0^t(\psi(\tau)-\psi_R)d\tau \qquad (8)$$

where δ_R is the actual rudder angle; ψ_R is the desired heading angle; K_i the integral parameter; K_R yaw gain constant; K_P a yaw rate gain constant (K_p>0, K_d>0, K_i>0); and t_r the time constant in rudder/pod activation.

2.2 Inclusion of pod effects in the mathematical model

An azimuthing podded drive is a highly attractive propulsion unit which combines the propulsion and steering actions of a ship, with a capability of 360° azimuthing, using an electric motor fitted inside the gondola part of the pod unit as shown in (Fig. 2). Thanks to electric motors being located outboard and power provided through either diesel or turbo generators inside ship's hull. This provides and improved onboard comfort, volume savings inside the hull and increased freedom in the general arrangement that can be obtained to enhance the design alongside the already well-established benefits in low speed manoeuvring. In order to illustrate the hydrodynamic characteristics of pod-driven ships, the afterbody arrangements of ships driven by a conventional twin-screw propeller system and a podded propulsor system are shown in Fig. 3.

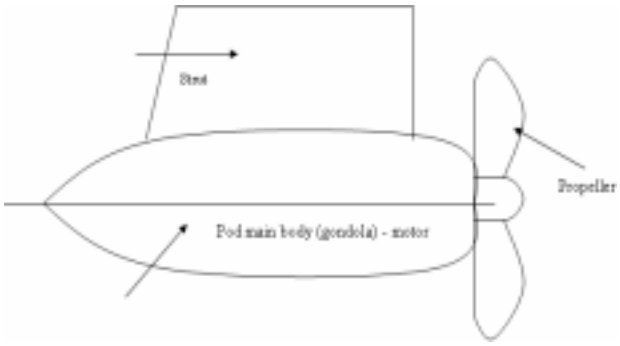

Figure 2 Sample body of a pod drive.

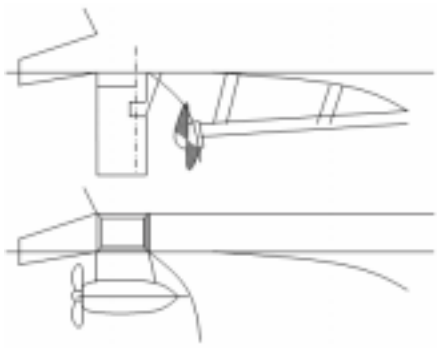

Figure 3 Conventional and azimuthing propulsion arrangements at aft part of a ship.

When a pod unit is slewed, unlike a conventional rudder which takes advantage of the accelerated propeller flow, the propeller slipstream is parallel to the pod for the most part and hence the pod remains at a zero angle of attack. As a result, although the pod propulsor has the superior advantage of vectoring the propeller thrust in any direction, the pod body (housing) without its propeller can only produce a lift proportional to the square of the ship forward speed, except the "straight ahead" condition. Within the same context although the pod housing should be considered as a single lifting surface subjected to the incoming flow, its two distinct components, which are the strut and gondola, suggest that the hydrodynamic characteristics of these parts can be developed separately and then combined by taking into account the interaction between them as precise as possible. Bearing in mind the fact that the interaction between the podded propulsors and the hull is relatively weak, particularly for high-speed applications as explored in this paper, there is a need to take into account this effect properly by taking into account the interaction amongst the pod housing, propeller and hull through properly selected interaction coefficients similar to the one for conventional rudders expressed in (1-2). Moreover, multitude number of the pods also requires taking this interaction effect between the pod units properly into account. In the following the motion equations given in (1) and (2) are modified to include the effect of the pod drives based upon the above background and concentrating on the 4 pods application (i.e. 2 fixed pod units located at the forward of the 2 steerable pod units), as shown in Fig 4. The following only states a brief summary of these modifications, the reader is referred to (Ayaz et al 2005) for the detailed derivations.

In Figure 4, T indicates thrust vector of pod induced forces and S indicates the side forces created by the propeller and the pod-housing unit. These terms can be obtained through lift and drag terms coefficients of the pod-unit.

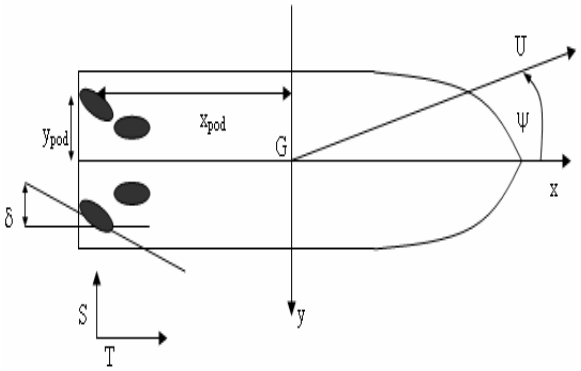

Figure 4 Locations and co-ordinate system for large high-speed pod-driven ship.

$$C_{D,L} = \frac{D,L}{0.5\,\rho\, A_{POD} U^{2}{}_{POD}} \tag{9}$$

where A_{POD} is effective pod area and U_{POD} is flow speed over the effective pod area. The pod drag and lift terms are determined based on open water characteristics can be expressed as:

$$\begin{aligned} L &= f(\beta_{POD}, \delta_{POD}, J_{POD}) = f(\alpha_{POD}, J_{POD}) \\ D &= f(\beta_{POD}, \delta_{POD}, J_{POD}) = f(\alpha_{POD}, J_{POD}) \\ \alpha_{POD} &= \beta_{POD} - \delta_{POD} \end{aligned} \tag{10}$$

where lift, L, and drag, D, forces are determined with respect to local drift angle of pod unit, β_{POD}, pod's deflection δ_{POD}, angle of attack α_{POD}, and advance coefficient J_{POD}. The pod angle of attack depends on whether a pod unit is a lee-ward or wind-ward one. The advance coefficient and subsequent thrust coefficient should be obtained from the total pod and propeller thrust force by taking into account propeller blade drag and pod-house unit resistance which can be expressed as:

$$K_{Tpod} = K_{Tpod+prp} + \Delta K_{blade} + \Delta K_{pod-house} \tag{11}$$

By combining (9) and (10) and (11), lift and drag coefficients can be finally written in the polynomial forms as:

$$\begin{aligned} C_D(\alpha) &= A_1 cos(B\alpha_{POD} - C) \\ &\quad + A_2 cos(2(B\alpha_{POD} - C)) + D \\ C_L(\alpha) &= K(J_{POD})\alpha_{POD} \end{aligned} \tag{12}$$

where constants A_1, A_2, C, D are obtained for different angle of attack and drift angle based on regression analysis. From the expressions given in (10), (11), (12) with a given local pod inflow angle (angle of attack), α_{POD}, lift and drag forces described in flow-oriented coordinate system can be transformed into thrust, T, and side force, S, units described in a ship-fixed coordinate systems. The pod-unit side force, S, is written as:

$$S = 0.5\rho\, A_{POD}\, U^{2}{}_{POD}\, f(\Lambda)\sin(\alpha_{POD}) \tag{13}$$

where $f(\Lambda)$ is the open water pod normal force coefficient, which is function of pod-strut aspect ratio, Λ, and it is described as:

$$f(\Lambda) = \frac{6.13\,\Lambda}{\Lambda + 2.25} \tag{14}$$

Finally, the relationship between hull and pod unit is described through the interaction coefficient, a_{Hpod} which is dependent upon advance coefficient J_{POD}, as seen from the previous formulations, and it is a significant parameter to describe side force and moment induced on hull by the pod units. The term could be expressed as:

$$\begin{aligned} a_{Hpod} &= a\,J_{POD} + b \\ where\ J_{POD} &= \frac{U_{POD}}{nD_P} \end{aligned} \tag{15}$$

The terms a and b, here, were identified from a regression analysis similarly to the ones in (9). In the absence of such information these terms can be taken based on open-water test results. With incorporation of the aforementioned terms and considering vector representation of the pod-induced forces in the lateral and vertical planes, the conventional formulation in (1) and (2) becomes (16) and (17) as below. Here, subscript pod denotes forces and moments caused by pod drive. Here, the last terms in X', Y', K', N' (surge, sway, roll and yaw) are given in similar notation to the conventional MMG model in (1) and (2). In

case of the fixed pods, pod-induced forces will be modified for the local drift angle of pod, β_{POD}, instead of the pod deflection (or slewing) angle, δ_{POD}:

$$
\begin{aligned}
&m(\dot{U}-VR) = -\iint_S p\mathbf{n_X}\,dS + X_H - S\sin(\delta) \\
&+(1-t_p)T\cos(\delta) \\
&m(\dot{V}+UR) = -\iint_S p\mathbf{n_Y}\,dS + \rho U \int_{\Gamma_X} \Phi_D n_Y\,ds + Y_H \\
&-(1+a_{Hpod})S\cos(\delta) + X'_{pod}\sin(\delta) \\
&m\dot{W} = -\iint_S p\mathbf{n_Z}\,dS + \rho U \int_{\Gamma_X} \Phi_D n_Z\,ds + Z_H
\end{aligned}
\tag{16}
$$

$$
\begin{aligned}
&(I_{xx}\cos^2\theta + I_{yy}\sin^2\theta)\dot{P} = -\iint_S p(\mathbf{r}\times\mathbf{n_{YZ}})\,dS \\
&+\rho U \int_{\Gamma_X} \Phi_D(\mathbf{r}\times\mathbf{n_{YZ}})\,ds + K_H + z_{Rpod}Y'_{pod} \\
&I_{yy}\dot{Q} = -\iint_S p(\mathbf{r}\times\mathbf{n_{ZX}})\,dS + \rho U \int_{\Gamma_X} \Phi_D(\mathbf{r}\times\mathbf{n_{ZX}})\,ds \\
&\quad + M_H \\
&(I_{xx}\sin^2\theta + I_{zz}\cos^2\theta)\dot{R} = -\iint_S p(\mathbf{r}\times\mathbf{n_{XY}})\,dS \\
&+\rho U \int_{\Gamma_X} \Phi_D(\mathbf{r}\times\mathbf{n_{XY}})\,ds + N_H - x_{pod}Y'_{pod}
\end{aligned}
\tag{17}
$$

2.3 Risk Control Options

In order to mitigate or prevent the occurrence of instability/capsizing of pod-driven ships, both operational and design risk control options were considered. The risk control options have been introduced either through operational guidelines recommended by IMO (1994) or the design options with ride control systems (active fin stabilisers for roll and yaw). Initially, the operational measures have thought to be preventive while the design measures through ride-control system are assumed mitigating. However during the course of the project, it was seen that they can be both mitigating and preventing. Yet, definitive conclusion to describe them as "preventive" will require more detailed analysis. The expression for the lift force term of a fin stabilizer is written, similar to pods and rudders, as:

$$L_{fin} = \frac{\partial C_L}{\partial \alpha}\cdot\alpha_{fin}\cdot\frac{1}{2}\cdot\rho\cdot U^2\cdot A_{Fin} \tag{18}$$

where L_{fin} is lift force of fin , α_{fin} is the incidence angle and A_{fin} is the effective fin area. Here, the lift curve slope in free stream is described as (Whicker & Fehlner, 1958):

$$\frac{\partial C_{Lfin}}{\partial \alpha} = \frac{1.8\cdot\pi\cdot\Lambda_{fin}}{1.8+\sqrt{\Lambda_{fin}^{\ 2}+4}} \quad (1/rad) \tag{19}$$

where, Λ_{fin} is the fin aspect ratio. The effect of activation on the fin characteristics is introduced through the control of the fin angle of attack. The method employs control parameter omitting fin servo and controller compensation coefficients to fin angle of attack, α_{fin}, as follows:

$$\alpha_{\text{fin}} = k_1\varphi + k_2\dot{\varphi} + k_3\ddot{\varphi} \tag{20}$$

where k_1, k_2, k_3 the roll angle, velocity, and acceleration gain values, respectively. Anti-yaw stabiliser induced forces will be measured with the similar control parameters used for the pod units.

3. NUMERICAL ANALYSIS

3.1 Validation Analysis

For the validation of the new mathematical model and further numerical analyses using the model, two ships; a high-speed ROPAX and a container ship, which are designed under FASTPOD project have been used (FASTPOD, 2005). The principal particulars of the vessels are given Table 1.

The FASTPOD ROPAX is propelled by four puller type pod units all equipped with 5.2

m propellers. Each pod absorbs approximately 27 MW power with the desired service speed approximately 38 knots. The forward pods are fixed and the aft pods are azimuthing for ship control.

FASTPOD Cargo is also propelled with four pod units all equipped with 6.5m propellers. Each pod absorbs approximately 36 MW power with the desired service speed approximately 35 knots.

Table 1. Principal particulars of FASTPOD ships

Parameter	FASTPOD ROPAX	FASTPOD Containership
L_{pp}	220 m	275 m
B (Beam)	30 m	30.0 m
D (Depth)	9.7 m	21.65 m
T (Draft)	6.8 m	10.30 m (design)
C_b	0.39	0.57
Δ	17600 t	49600 t (design)
LCG	-5.71 m (aft)	-7.2 m (aft)
VCG	14.60	13.60 (design)
V (speed)	38 knots	35 knots

For the validation analysis of the numerical model, free-running model test results for ROPAX vessel were used (Trägårdh et. al, 2004). These tests were conducted in the Marine Dynamics Laboratory facility at SSPA in Sweden. The four pod propellers were driven mechanically from inside the hull and assume a constant torque model. For the containership, a series of seakeeping model experiments, which were carried out at model basin facilities of CTO, Poland, are used since they were specifically focused on the occurrence of parametric resonance, of which this type of vessels are particularly vulnerable, in long-crested seas (Bednarek & Kanar, 2005).

For the ROPAX vessel, significant single amplitude, which has been measured as twice the standard deviation of each motion for time series in 6 DOF, was used for comparison with model tests (Fig. 5). The comparison of the measurements with the predictions from the enhanced mathematical model displayed very good correlation as shown in (Fig. 5).

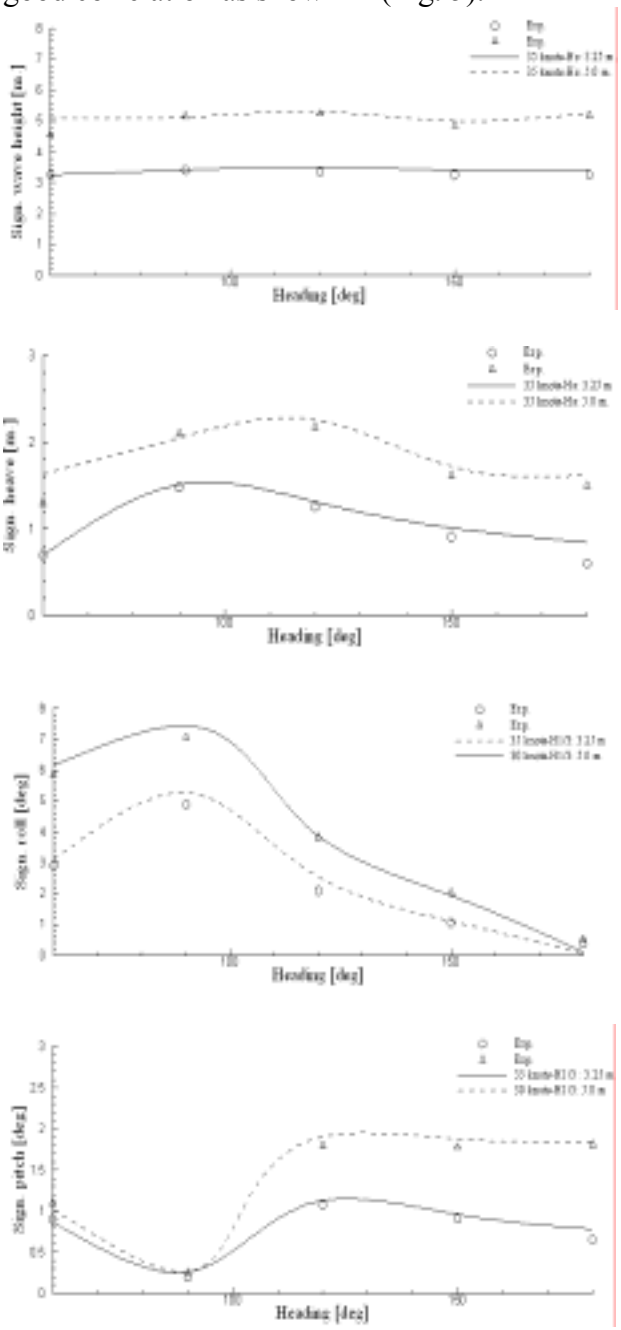

Figure 5 The significant single amplitude of the identified parameters for ROPAX.

The similar validation analysis has been also conducted for so-called "composed irregular" waves concept where, as the name indicates, a random wave is created with number of different frequency regular wave components. The numerical wave model has followed more "regular-like" cases where the

model was run to simulate relatively large wave amplitudes in beam seas. A test case for such simulation is illustrated in Figure 6.

In this analysis, although quantitative agreement seems to be obtained there is significant qualitative differences due to differences between numerical runs which was carried out with single wave period while experiments was conducted as two different regular wave runs.

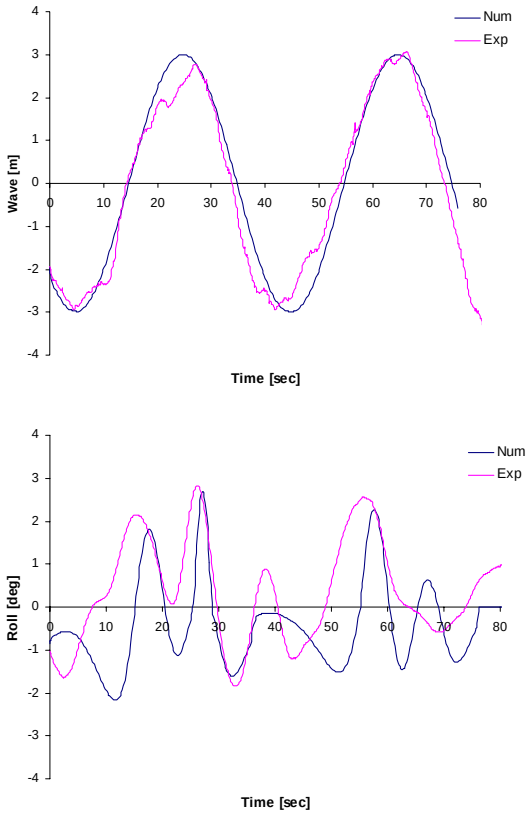

Figure 6 Composed irregular wave analysis.

The unique design and loading/stability characteristics of containership investigated required greater attention for the investigation of possible dangerous conditions that the ship may have faced to during the course of voyage. These were noted during the manoeuvring trials of ship model in open lake in which the large static heeling due to low GM enforced to abandon the turning circle tests for the maximum rudder angle (35 degrees) despite the superior turning and directional control abilities observed during the tests. Therefore, the dedicated seakeeping model tests were carried out at the CTO model basin for the investigation of auto-parametric rolling of the containership in long-crested seas (Bednarek & Kanar, 2005). Parametric roll test matrix has been created in accordance with the assumption of following resonance condition:

$$\omega_\phi = \frac{1}{2}\omega_e n \,(n = 1,2,...) \tag{21}$$

where ω_e, is encounter frequency and ω_φ is natural roll frequency. The region of principal resonance has been shown from the solution of linear Mathieu equation for unforced roll motion which can be written as:

$$\ddot{\phi} + 2(\frac{2N}{T})\dot{\phi} + \omega_0{}^2\left[1 - \frac{\Delta GM}{GM_0}(\cos\omega_e t)\right]\phi = 0 \tag{22}$$

where the term $\Delta GM/GM$ (Θ_P) indicating fluctuating GM yields to:

$$\Theta_P = \frac{\Delta GM}{GM} = \frac{GM_{TROUGH} - GM_{crest}}{2GM_0} \tag{23}$$

Here, GM_0 represents the metecentric height in calm water while N in (22) is non-dimensional roll damping coefficient. In this study N term has been obtained using the roll decay tests. The relationship in (21)-(23) has been illustrated by the well-known Ince-Strutt stability diagram of the solutions of Mathieu's equation (Fig. 7).

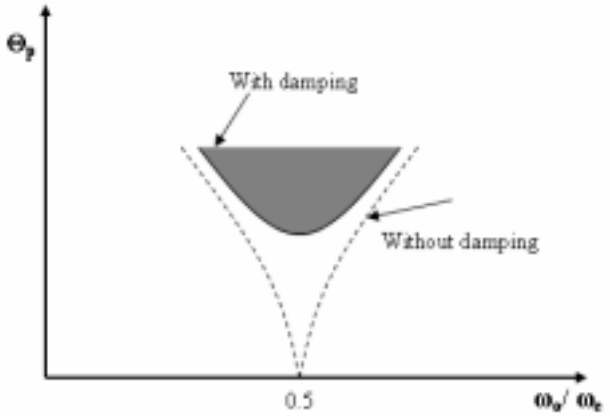

Figure 7 Ince-Strutt Diagram.

Moreover, the GZ (righting arm) curve of the vessel is plotted in Fig. 8 for wave trough

and wave crest as well as in the calm waterfor the resonance condition shown in Fig. 7.

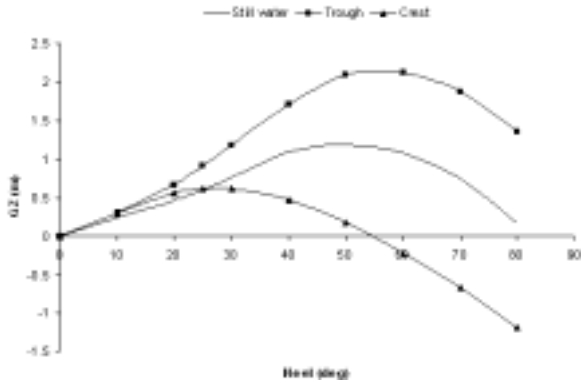

Figure 8 Containership GZ curve in calm water and waves for resonance condition.

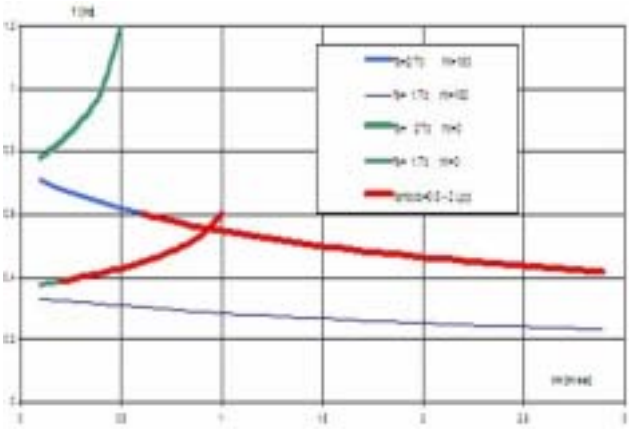

Figure 9 The diagram for speed (V) and wave frequency (f) in model basin where red line depicts parametric rolling zone (Bednarek & Kanar, 2005).

The boundary for occurrence of parametrical rolling in design condition of container ship is given in Figure 9.

The validation results of the enhanced mathematical model using all 6-DOF for the prediction of parametric roll behaviour of the container ship in steep regular waves are presented in Fig. 10 and 11.

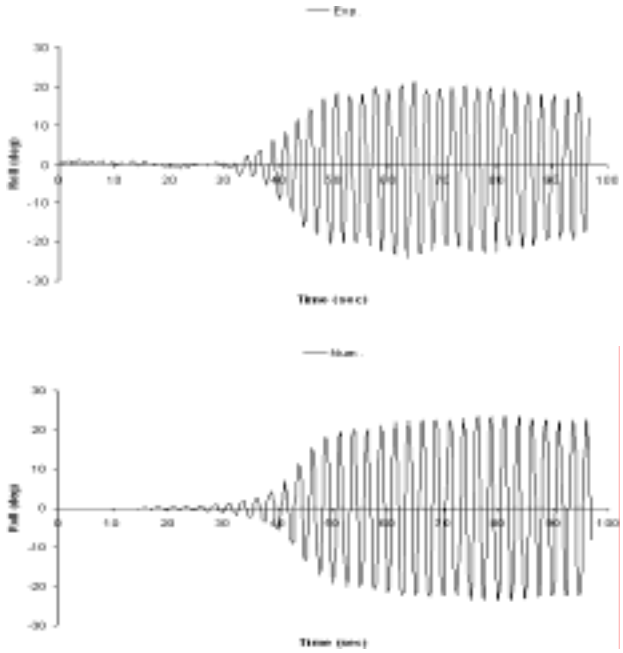

Figure 10 Parametric resonance for containership. Wave length/L_{pp}=1.0, H=7.08 m., ψ=180°, V=14.9 knots (model scale)

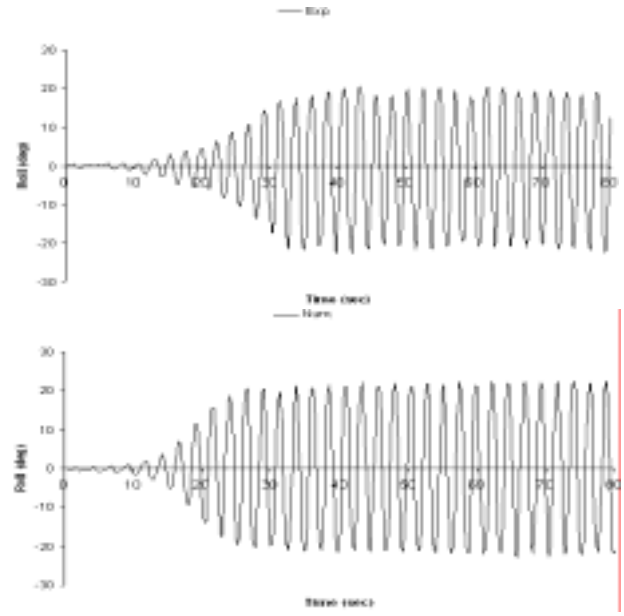

Figure 11 Parametric resonance for containership. Wave length/L_{pp}=1.15, H=7.132 m., ψ=180°, V= 12.4 knots (model scale).

The prediction appears to be reasonable despite some initial differences leading up to parametrical build-up due to experimental set-up which aim to prevent capsize during the trials.

3.2 Parametric Analysis

Following the validation analysis, parametrical investigation was carried out to identify susceptibility of pod-driven high speed ships that may lead to dangerous conditions in waves. This investigation was further extended to elaborate on the possible design or other operational risk control options. The latter option can be implemented either through operational guidelines recommended by IMO (1995) or the numerical simulation with ride control systems (active fin stabilisers for roll and yaw). In order to demonstrate the effectiveness of the fin stabilisation system, which has been opted for this investigation, the comparison of the roll motion amplitudes with and without the stabilisers is shown in Fig. 12.

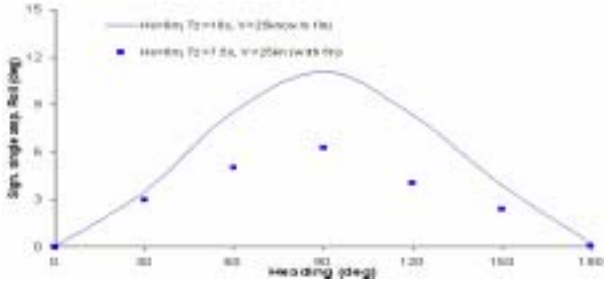

Figure 12 Comparison of roll motion of ROPAX with and without active roll fin stabilisers (rate 10°/sec).

Some of the instability and capsizing conditions identified by the numerical model are presented in Figs. 13-14. It is found that in the normal service speed conditions the ROPAX ship can be susceptible to some of dangerous conditions: surf-riding when captured by a single wave in following seas (Fig.13) the capsizing is also observed further towards to quartering seas.

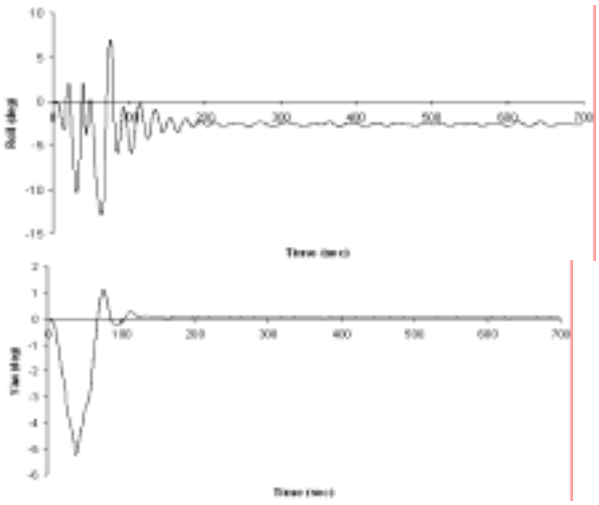

Figure 13 The occurrence of surf-riding for ROPAX in steep regular wave, λ/L_{pp}=1.0, H=8 m., ψ=0°, V=35 knots.

Accordingly, the analysis in random waves, where more realistic sea conditions and less number of successive steep waves result in less likelihood of such dangerous conditions comparing to regular waves, have indicated yaw instability in some conditions. The anti-roll and yaw stabilisers were effective in this (Fig.14).

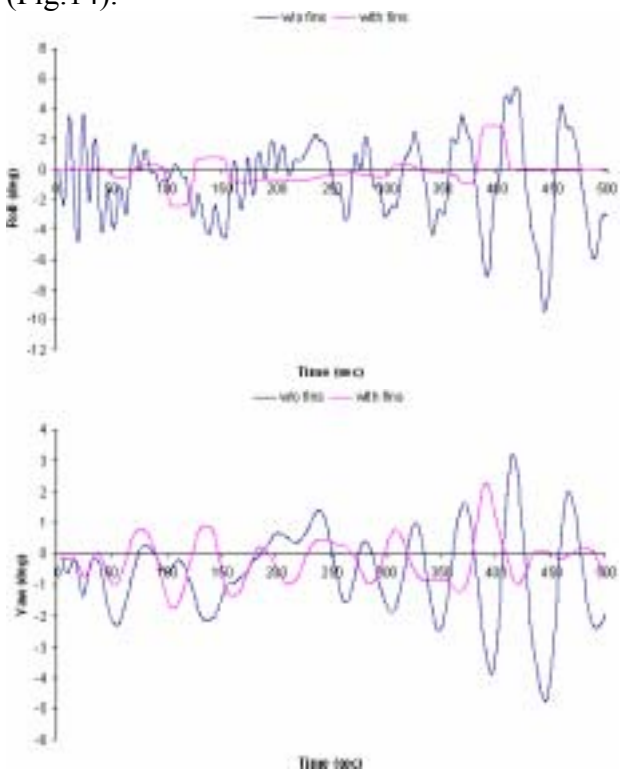

Figure 14 The occurrence of large build-up of yaw for ROPAX in random waves, Hs=8 m., T_o=10.2 sec., ψ=30°, V=30 knots.

For further investigations of the containership critical motion behaviours, the conditions similar to model tests have been chosen from annual weather forecast of North Atlantic route where the vessel will be operating. The recommendations by IMO (1995) have been applied through changing course and speed.

It is seen that the ship is out-of-phase with resonance conditions which were observed in first condition (Fig. 15) and experienced the roll motions in lesser amplitudes in very high seas (Fig. 16). However, it is should be noted that phasing-out of this motion should not be interpreted as the prevention since important coupled effects such as cargo shifting etc… are not taken into account. The steady wind speed of 40 knots has been assumed for all numerical simulations. An operability diagram for the parametric rolling and slamming occurrence for containership is illustrated in Figure 17.

The stability of analysis pod-driven high speed craft has indicated some safety-critical conditions that could be observed although rather seldom, in the actual voyages. These conditions could be attributed to hull form which is shaped to accommodate pod units at the aft. In the design of pod system, the gondola and strut shapes have been chosen to be slender and rather long in order to achieve optimum propulsive efficiency and minimum cavitation danger. The selection process was also largely influenced by existing motor technology to accommodate such a large power per unit for the high-speed requirements of these ships (FASTPOD, 2005).

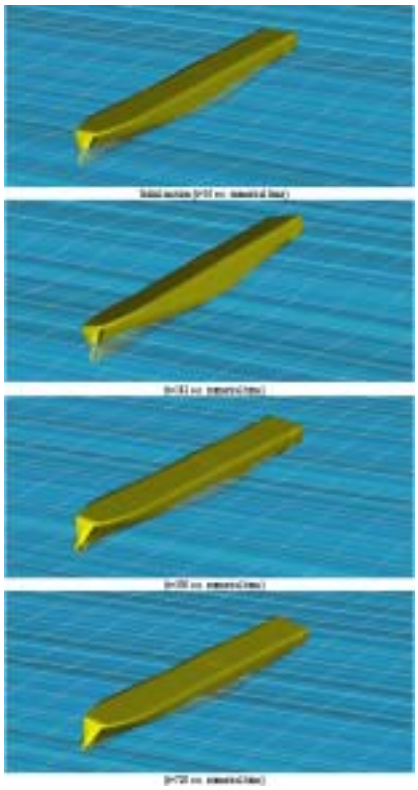

Figure 15 Numerical simulation of containership V= 15.14 knots, Hs=9.32 m., T_o=14.89 sec., ψ=0°.

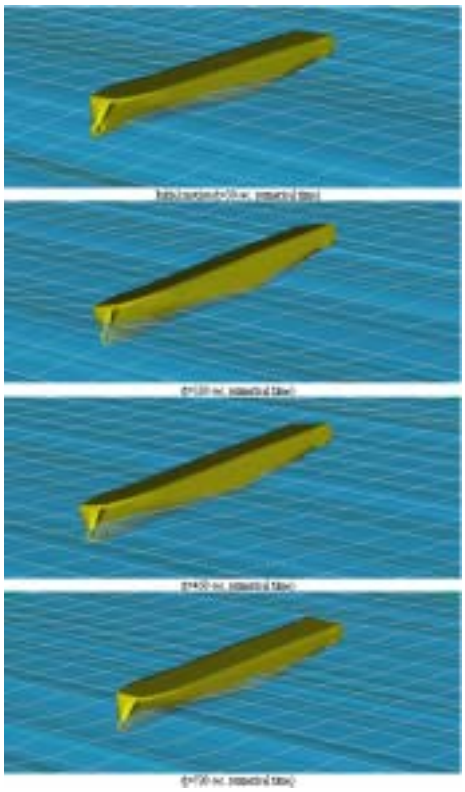

Figure 16 Numerical simulation of containership V= 16.155 knots, Hs=9.32 m., T_o=14.49 sec., ψ=15°.

Furthermore, as reported by Woodward et al (2005), the extreme steering can exert large manoeuvring induced side loads of spike nature on the entire pod units due to their high acceleration dependency. These loads do not only cause structural concern but can also induce large initial heeling which is further

safety-critical issue for pod driven ships. A detailed study discussing these effects is presented in an accompanying paper by the authors as reported in Ayaz et al (2006).

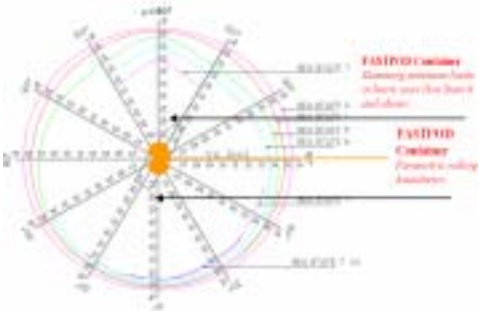

Figure 17 Parametric rolling (circles) and slamming boundaries (black arrows) on the attainable ship speed diagram under wave heading and wind direction for containership (Sea State 6 and above).

4. CONCLUSIONS

An existing 6 DOF non-linear numerical model has been enhanced for the simulation of motion control and stability analysis of pod-driven high-speed and large ships in waves. The enhancements have been accomplished by introducing the thrust and lateral force components of multitude of azimuthing and fixed pod drives in combination.

The numerical results have been verified against the experimental results for high-speed ROPAX and containership, which are designed under the EC funded collaborative project FASTPOD and displayed satisfactory agreement in overall.

It was observed from seakeeping analyses that large pod-driven vessels display favourable characteristics in high-speed and potentially dangerous operational conditions. However, large aft area to accommodate the multitude of large pod units could expose the ship to parametric build up of yaw-roll combination. This has been realised for extreme steep waves in low encounter frequency conditions which is suitable for the dangerous conditions like surf-riding and broaching. Many risk control options such as reducing the speed and changing the course of vessel could be effective. Moreover, as design options, the effect of ride control systems has been investigated and it is shown that many dangerous conditions or instabilities can be mitigated by applying ride control systems. The shape of after body modification of the hull due to pod propulsion as well as bow flare requirement on a loading-critical ship type, such as container, the parametrical rolling or similar dangerous conditions have been observed near to pure following and head seas conditions although these are confined to very extreme cases.

It is thought that many of these problems associated with the container ship type could be caused due to very low GM to accommodate the targeted cargo as well as heavy pods in the aft. Anti-roll tanks can be proposed to tackle this problem as well as the aforementioned operational steps can be undertaken.

Based on the parametrical analysis undertaken during the course of this study, it could be argued that the improvement in motor technology and reduction in motor sizes and eventually pod sizes, will positively affect the viability of large pod-driven high-speed ships in terms of stability and control in waves.

Finally, it is believed the modified numerical model provides satisfactory results for the analysis of dynamic stability of high-speed, large podded ships by multiple large pod units in waves and it could be a useful tool during the preliminary design process for such vessels.

5. ACKNOWLEDMENTS

This study was carried out under European Commission research project FASTPOD (GRD2-2001-50063). The authors wish to thank all 17 partners of FASTPOD project for the prompt collaboration during the whole development of the project.

6. REFERENCES

Ayaz, Z., Turan, O., Vassalos, D., 2004, "Manoeuvring Aspects of Pod Driven Ships" Proceedings of First International Conference on Technological Advances in Podded Propulsion (T-POD), Newcastle upon Tyne, Atlar et al., University of Newcastle Publication, UK, pp. 135-152.

Ayaz, Z., Turan, O., Vassalos, D., 2005, "Manoeuvring and Seakeeping Aspects of Pod Driven Ships" Journal of Engineering for the Maritime Environment-Proceedings of the Institution of Mechanical Engineers Part M, Vol. 219, pp. 77-91.

Ayaz, Z, Vassalos D., Spyrou, K.J., 2006 (in press), "Manoeuvring Behaviour of Ships in Extreme Astern Seas", Ocean Engineering.

Bednarek, A., Kanar, J., 2005 "Cargo Vessel-Results of Parametric Roll Model Tests" Project Report (FASTPOD-GRD2-2001-50063), *Commercial in confidence*, CTO, Poland.

FASTPOD, "Fast Ship Application for Pod Drives", European Commission RTD Project, GRD2-2001-50063, 2002-2005.

IMO, 1995 "Guidance to the Master for Avoiding Dangerous Situations in Following and Quartering Seas, MSC Circular 707, IMO Publication, London, UK.

Inoue, S., Hirano, M., Kijima, K. and Takashina, J., 1981 "A Practical Calculation Method of Ship Manoeuvring" International Shipbuilding Progress, Vol. 28, No. 324, pp. 207-222.

ITTC, 2005 "The Specialist Committee on Azimuthing Podded Propulsion. Final Report and Recommendations to the 24th. ITTC", Proceedings of 24th ITTC, University of Newcastle upon Tyne Publication, Vol. 2, pp. 543-600, Edinburgh, UK

OPTIPOD "Optimal Design and Implementation of Azimuthing Pods for Safe and Efficient Propulsion of Ships" European Commission RTD Project, GRD1-1999-10294, 2000-2003

Toxepus, S., Loeff, G., 2002, "Manoeuvring Aspects of Fast Ships with Pods" Proceedings of Euro conference on high-speed performance marine vehicles, Bergen, Norway, pp. 392-406.

Tragardh, P., Hua, J., Lee-Andersen, M., 2004 "Development of Fast ROPAX, Seakeeping and Wave wash model tests, Free-running manoeuvring model tests" Project Report (FASTPOD-GRD2-2001-50063), C*ommercial in confidence*, SSPA, Sweden AB.

Van Terwisga, T., Quadvlieg, F., Valkhof, H., 2001, "Steerable Propulsion Units: Hydrodynamic Issues and Design Consequences" Paper written on the occasion of 80th anniversary of Schottel GmbH & Co, Germany.

Whicker, L.F., Fehlner, L.F., 1958 "Free stream characteristics of a family of low aspect ratio all moveable control surfaces for application to ship design, David Taylor Model Basin Report, No:933, USA.

Woodward, M.D., Atlar. M., Clarke, D., 2005, "Manoeuvring induced loads on fast pod drives" FAST 2005, St. Petersburg, Russia